ACS OMEGA

Open Access

http://pubs.acs.org/journal/acsodf

Article

Effect of Sc on the Wettability of ER5356 Welding Wires and the Porosity of Deposited Metal

Haolin Zeng,[‖] Zhuo Wang,[‖] Donggao Chen, Hua Ding, Wenjing Yang,* Liangchao Ma, and Yu Lu

Cite This: *ACS Omega* 2024, 9, 14255−14261

Read Online

ACCESS | Metrics & More | Article Recommendations

ABSTRACT: In this study, Al−Mg and Al−Mg−Sc ER5356 welding wires were adopted, and the effects of the Sc element on the wetting behavior of the molten metal and the porosity of the deposited metal were investigated. Al−Mg−Sc and Al−Mg welding wires exhibit wetting angles of 17.2 and 12.4°, respectively, and their porosities of deposited metal were 0.885 and 0.454%, respectively. Adding the Sc element to ER5356 welding wires reduced the surface tension and then increased the pore difference pressure, wettability, and spreadability of the molten pool, which is beneficial for pore overflow. Besides, adding Sc elements could increase the molten droplet size and the metallic vapor recoil for the ER5356 wire and then stabilize droplet transfer.

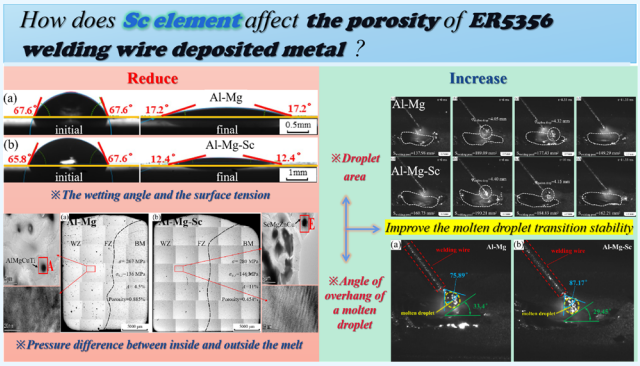

1. INTRODUCTION

Aluminum alloys play important roles and have a wide range of uses in industrial manufacturing, especially the 7xxx series aluminum alloy (Al−Zn−Mg−Cu series alloy). Because of the advantages of its high strength, toughness, and good weldability, the 7A52 alloy is widely used in load-bearing structures for vehicles.[1−3] The Al−Mg alloy is typically used as a filler wire to ensure that 7A52 components meet the welding toughness, strength, and noncracking requirements.[4,5] The Al−Mg series of alloys cannot be strengthened by heat treatment. Therefore, microalloying elements, such as V, Cr, Zr, Ti, Sc, etc., are added to improve the microstructure and mechanical properties of the material.[6−8] Soviet scientists established that the Sc element had the most significant impact on the microstructure and properties of aluminum alloys.[9,10] In the past few decades, Russia, Japan, the USA, Canada, Europe, and other countries have studied the effects of Sc on aluminum alloys, which are widely used in aviation, aerospace, marine transportation, and other industries.[11,12] The primary Al_3Sc particles can refine the grains during solidification, and the scattered secondary Al_3Sc particles can prevent recrystallization and dendrite formation. The Al_3Sc alloy can improve performance and reduce casting defects for welding joints.[13−16]

Based on the solid joint achieved from the Al−Mg−Sc welding wire, researchers have illustrated the effect of Sc on improving the microstructure and mechanical properties. However, the influence of Sc elements on molten metal during the Al−Mg−Sc welding process has not been studied.

The welding wire cools from the weld pool to the deposited metal, and its surface tension determines how the melt reacts and how the droplet wets and spreads on the base metal (BM), which influences the quality of the weld joint. Additionally, the melting characteristics of metals are determined by their chemical composition. According to Deng et al., during aluminum alloy laser wire-filled welding, as the Mg content of the welding wire increases, the surface tension gradually decreases.[17] The recoil pressure, gravity, and surface tension create a downward force that causes a more severe disturbance to the keyhole, resulting in more porosity in a welding zone. There are no studies on the wetting angle of a molten welding wire and the influence of Sc elements on wettability. This paper characterizes the wetting angle of the ER5356 welding wire and then investigates the influence mechanisms of Sc elements on the wettability of ER5356 welding wires and the porosity of the deposited metal.

2. MATERIALS AND METHODS

2.1. Measurement of Contact Angle. Al−Mg and Al−Mg−Sc welding wires with 1.6 mm diameter were used in this study. The welding wire composition at the initial smelting stage is designed as Al−5Mg−0.2Mn−0.15Cr−0.15Ti−0/0.2Sc. Welding wires have uneven element compositions due to casting, burning loss, drawing, and other processes. The

Received: December 14, 2023
Revised: February 23, 2024
Accepted: February 28, 2024
Published: March 12, 2024

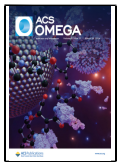

high-temperature contact angle of the welding wire was tested by a DSAHT17C tester using the drip method. A 20 g welding wire was heated to 660 °C in an argon gas atmosphere, extruded from a graphite tube, and dropped on 7A52 BM (30 mm × 30 mm × 10 mm).

The surface roughness is less than 10 μm, and the spreading behavior of the droplets was measured with Digitizer software. Table 1 shows the composition of the tested welding wire and 7A52 BM.

Table 1. Compositions of the Experimental Materials (wt %)

materials	Mg	Mn	Cr	Ti	Sc	Al
Al−Mg wire	4.8	0.18	0.13	0.12	0	bal.
Al−Mg−Sc wire	4.9	0.17	0.15	0.14	0.17	bal.
7A52 BM	3.1	0.28	0.19	0.05	0	bal.

2.2. High-speed Photography of Molten Droplet Transition. Melt inert-gas (MIG) welding is adopted, and the shielding gas for the welding seam is 99.99% pure argon; the schematic of welding is shown in Figure 1.

The welding electric current, voltage, and speed are 180 A, 20 V, and 0.6 m·min^{-1}, respectively. The drop-transfer process in welding was recorded by an Optronics/Cyclone-2-2000-M high-speed camera. Upon welding, the cross-sectional specimens of the deposited metal were acquired by wire cutting, and then the porosity of the samples was observed after grinding and polishing.

2.3. Transmission Electron Microscopy (TEM) Sample Preparation. Samples of the Al−Mg and Al−Mg−Sc deposit metal were prepared for transmission electron microscopy (TEM) characterizations as follows. First, the samples were roughly ground and hand-ground with sandpaper on a mechanical pregrinding machine to obtain thin slices of about 70 μm thickness. The flakes were punched into thin disks with a diameter of 3 mm by using a punching machine. The samples were electrolyzed and double-sprayed by a TenuPol-5 automatic electrolytic double-spraying equipment, with an electrolyte volume ratio of nitric acid/methanol = 1:3, a voltage of 15 V, a current of 40−60 mA, and a transmittance of 80−100. The electrolytic double-spraying equipment is shown in Figure 2a.

Before the TEM observation, the thickness of samples was reduced through ion-beam thinning using a Gatan695.C/PIPSII ion-thinning instrument, with the voltage set at 3 V and the angle at ±4°, to ensure further the appearance of thin zones in the samples, to remove oxidized layers, and to increase the success rate of the TEM sample preparation. The ion-thinning equipment is shown in Figure 2b. The high-resolution TEM and TEM microstructures of the Al−Mg and Al−Mg−Sc deposit metals were observed on a Talos F200S G2 transmission electron microscope. The specific TEM equipment is shown in Figure 2c.

3. RESULTS AND DISCUSSION

3.1. Porosity of the Deposited Metal. Images of the cross sections of the deposited metal for Al−Mg and Al−Mg−Sc samples were observed by transmission electron microscopy (TEM), as shown in Figure 3. The images show deposited metal and pores in the macrostructure and Al grains with a precipitate inside in the microstructure. IPP was used to calculate the porosity of the Al−Mg and Al−Mg−Sc samples, and the porosity values were 0.885 and 0.454%, respectively (Table 2). In the Al−Mg−Sc cross-sectional specimen, pores are fewer in number and smaller in size. Therefore, adding the Sc element to the ER5356 welding wire significantly reduced the pore quantity and size of the deposited metal.

3.2. Wetting Angle in Equilibrium. Figure 4a,b illustrates the initial and final wetting conditions of 20 g of Al−Mg wire and Al−Mg−Sc wire melts after wetting on the 7A52 substrate. The initial wetting angles are 67.6 and 65.8°, and the final wetting angles are 17.2 and 12.4°, respectively. As both wires could wet the 7A52 BM, the Al−Mg−Sc wire exhibited a smaller wetting angle and a better wetting effect than the Al−Mg wire.

3.3. Analysis of the Wetting Behavior of the Melt. The surface tension (σ_{lg}) of the aluminum element is 0.91 N·m^{-1} when it reaches the melting point, and σ_{sg} is 1.91 N·m^{-1} at 20 °C.[18] According to the Young equation.[19]

$$\cos\theta = (\sigma_{sg} - \sigma_{sl})/\sigma_{lg} \quad (1)$$

σ_{sg}, σ_{sl}, and σ_{lg} denote the interfacial tension at the solid−gas, solid−liquid, and liquid−gas interfaces. According to Figure 4, $\cos\theta_{Al-Mg}$ is 0.955 and $\cos\theta_{Al-Mg-Sc}$ is 0.977. As the two wires exhibit different wetting properties at the same 7A52 BM surface state and experimental temperature, it can be assumed that the wetting behaviors of the wires were affected by their composition.

The study by Molina et al.[20] states that the wetting angle of pure Al element under vacuum conditions is 81°, much higher than the 17.2 and 12.4° obtained here, and the surface tension of the Al element under melting conditions can be expressed as follows

$$\sigma_{lg} = 0.883 - 0.185(T - 660) \quad (2)$$

The unit of σ_{lg} is N·m^{-1}, and the unit of T is °C.

$$\cos\theta_{Al} = (\sigma_{sg} - \sigma_{sl})/\sigma_{lg\,Al} = 0.156 \quad (3)$$

$$\cos\theta_{Al-Mg} = (\sigma_{sg} - \sigma_{sl})/\sigma_{lg\,Al-Mg} = 0.955 \quad (4)$$

$$\cos\theta_{Al-Mg-Sc} = (\sigma_{sg} - \sigma_{sl})/\sigma_{lg\,Sc} = 0.977 \quad (5)$$

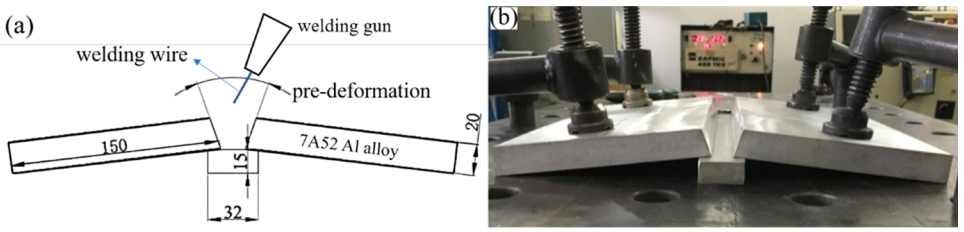

Figure 1. Schematic of welding: (a) assembly schematic and (b) actual assembly drawings.

https://doi.org/10.1021/acsomega.3c10018
ACS Omega 2024, 9, 14255−14261

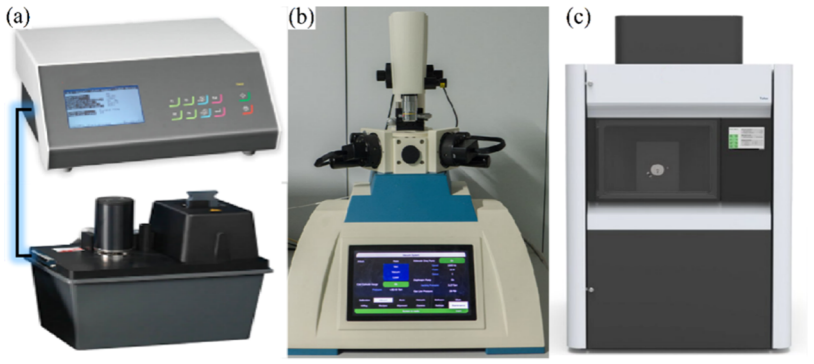

Figure 2. TEM experimental apparatus: (a) automatic electrolytic double-spraying equipment, (b) Gatan695.C/PIPSII Ion thinning instrument, and (c) Talos F200S G2 TEM.

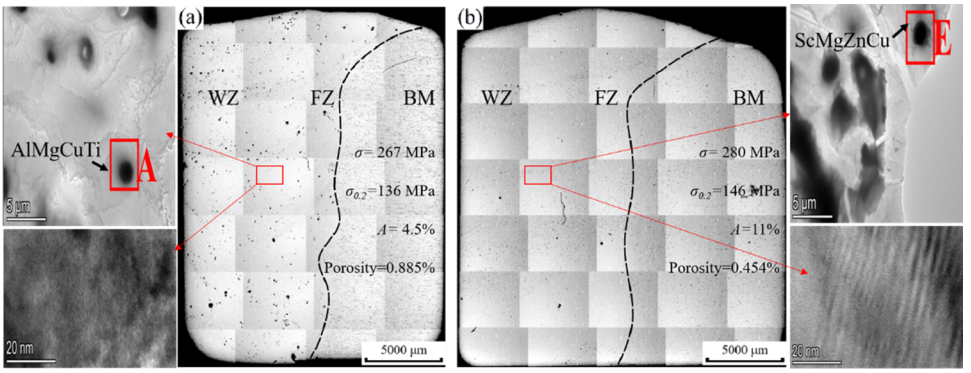

Figure 3. Cross-sectional micromorphology of the deposited metal: (a) Al−Mg wire and (b) Al−Mg−Sc wire.

Table 2. Wire Molten Metal Porosity Distribution Rate of Two Types of Welding Wires

welding-wire	welding zone	stomatal zone	porosity
Al−Mg	424994	3761	0.885%
Al−Mg−Sc	534481	2424	0.454%

The results of eqs 3−5 show that the addition of an alloying element such as Sc drastically reduces the surface tension of the melt, which leads to the improvement of its wettability.

The part of the melt in contact with the surface of the specimen is similar to that of a hemisphere. Therefore, according to Figure 4c, it can be concluded that

$$\cos\theta = (R - h)/R \tag{6}$$

In the formula, R is the radius of the spherical crown after melt spreading, h is the height of the spherical crown, and h_{Al-Mg} and $h_{Al-Mg-Sc}$ were measured by the drip method to be 0.243 and 0.193 mm, respectively.

Equation 7 is based on the simultaneous solution of eqs 1−6

$$\sigma_{sl} = \sigma_{sg} - \sigma_{lg}\{(R - h)/R\} \tag{7}$$

The values of $\sigma_{sl\ Al-Mg}$ and $\sigma_{sl\ Al-Mg-Sc}$ are calculated as 1.041 and 1.021 $N{\cdot}m^{-1}$, respectively.

$$V = \pi h(h^2 + 3r^2)/6 \tag{8}$$

$$A_0 = A_{sg} + A_{lg} \tag{9}$$

$$A_{lg} = \pi(r^2 + h^2) \tag{10}$$

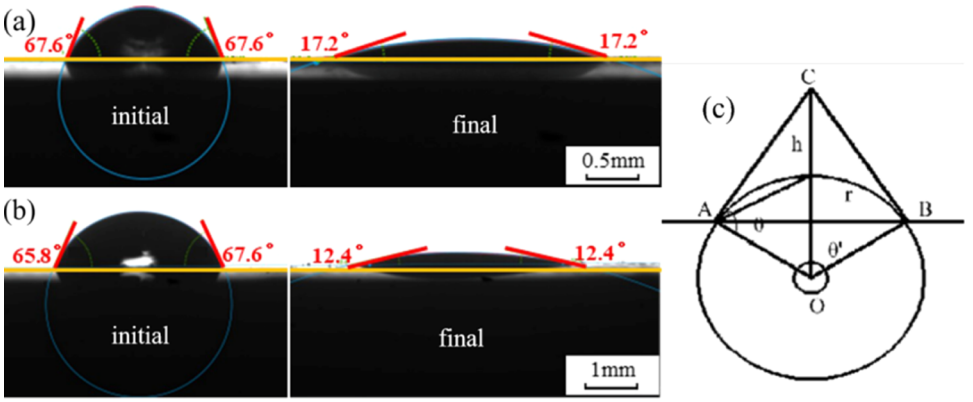

Figure 4. Wetting angle: (a) Al−Mg wire and (b) Al−Mg−Sc wire. (c) Schematic diagram of cross-sectional melt spreading.

https://doi.org/10.1021/acsomega.3c10018
ACS Omega 2024, 9, 14255−14261

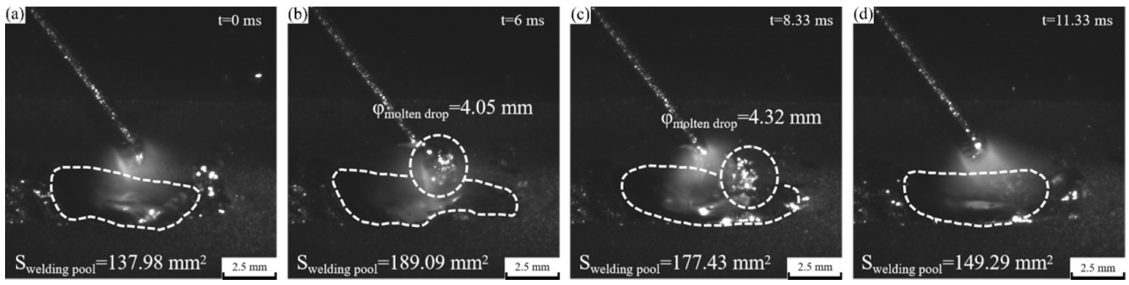

Figure 5. Molten droplet transition form of the Al−Mg wire.

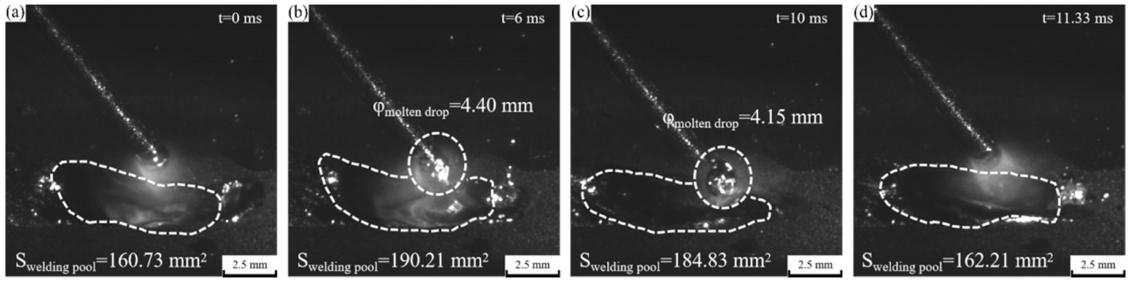

Figure 6. Molten droplet transition form of the Al−Mg−Sc wire.

A_{sg}, A_{sl}, and A_{lg} denote the contact area between solid−gas, solid−liquid, and liquid−gas interfaces. A_0 is the surface area of the base material, and r is the radius of the spherical crown.[21]

The equilibrium volumes of molten droplets were measured as V_{Al-Mg} = 0.665 mL^3 and $V_{Al-Mg-Sc}$ = 0.756 mL^3, according to Figure 4. The simultaneous solution of eqs 8−10 yields r_{Al-Mg} and $r_{Al-Mg-Sc}$ values of 1.312 and 1.575 mm, respectively, and $A_{0\ Al-Mg}$ and $A_{0\ Al-Mg-Sc}$ values of 11.004 and 15.705 mm^2, respectively.

As the melt is fully spread out, the energy is in its lowest state and the system reaches equilibrium. In this case, the energy balance equation is given below[22]

$$E_{total} = \sigma_{lg}\pi(r^2 + h^2) + \sigma_{sg}(A_0 - \pi r^2) + \sigma_{sl}\pi r^2 \quad (11)$$

$E_{total\ Al-Mg}$ and $E_{total\ Al-Mg-Sc}$ were calculated to be 20.943 and 29.924 kJ, respectively.

In the Young−Laplace equation[23,24]

$$\Delta P = Ps = 2\sigma_{sl}/R \quad (12)$$

ΔP is the pressure difference between the inner and outer interfaces of the molten droplets in equilibrium. By incorporating the above results into eq 12, ΔP_{Al-Mg} and $\Delta P_{Al-Mg-Sc}$ were calculated to be 0.086 and 0.106 MPa, respectively. Two wires were tested in the same atmospheric pressure environment. The pressure difference between the inside and the outside of the melt formed by the Al−Mg−Sc wire is higher than that of the Al−Mg wire. The gas bubbles were easier to rupture and overflow out of the Al−Mg−Sc molten metal. As a result, the Al−Mg−Sc-deposited metal has a lower porosity than the Al−Mg sample.[25]

$$F = \sigma_{lg}C \quad (13)$$

$$W_i = -\sigma_{lg}\cos\theta \quad (14)$$

Here F is the downward gravitational force on the melt, C is the scope of force action, and W_i is the wetting work.

The average radii of the Al−Mg and Al−Mg−Sc melts were measured to be 1.34 and 1.59 mm, respectively, according to Figure 4. The gravitational forces on the substrate surface were calculated to be 5.15 × 10^{-6} and 7.24 × 10^{-6} N for the Al−Mg and Al−Mg−Sc wires, respectively. The values of the wetting work of the Al−Mg and Al−Mg−Sc wires were 0.869 and 0.889 J, respectively.

Apart from considering the wetting properties of the melt, the adsorption properties of the substrate itself for the melt should also be considered. According to Li's mathematical model,[26] the adsorption working at the interface between the melt−liquid surface (E_{lg}) and the liquid−solid surface (E_{sl}) can be expressed as follows

$$E_{lg} = (\sigma_{lg}^{Al-Mg-Sc} - \sigma_{lg}^{Al})S_m - m\lambda \quad (15)$$

$$E_{sl} = E_{lg} + (W_{ad}^{Al} - W_{ad}^{Al-Mg-Sc})S_m \quad (16)$$

$$W_{ad} = \sigma_{lg}(1 + \cos\theta) \quad (17)$$

In the formula, S_m is the interfacial area occupied by the monolayer melt atoms, m is a structural parameter of about 0.25, and λ is the mixing enthalpy of the molten droplet after uniform distribution of the Sc element. The mixing enthalpy of Al−Sc is 38 kJ·mol^{-1} and that of Al−Mg is −2 kJ·mol^{-1}, according to the Miedema model.[27,28] $W_{ad}^{Al-Mg-Sc}$ and W_{ad}^{Al} are the adsorption working at the interface between Al−Mg−Sc and Al BM, which can be derived from eq 18.[29]

$$S_m = cN^{1/3}V^{2/3} \quad (18)$$

Here c is the dense lattice geometric factor constant of 1.091, N is the Avogadro constant, and V is the molar volume of the melt.

Based on the results of the drip method, the molar volumes of Al−Mg and Al−Mg−Sc wires were 10.685 and 10.733 mL·mol^{-1}, respectively. The S_m^{Al-Mg} and $S_m^{Al-Mg-Sc}$ values were calculated as 4.46 × 10^4 and 4.48 × 10^4 mm^2·mol^{-1}, respectively. On substituting them into eqs 15 and 16, the E_{lg} and E_{sl} for Al−Mg wires are 1.205 and −33.805 kJ·mol^{-1} and those for Al−Mg−Sc are 1.219 and −34.853 kJ·mol^{-1}, respectively. According to the calculated results, adding the Sc

https://doi.org/10.1021/acsomega.3c10018
ACS Omega 2024, 9, 14255−14261

element leads to an increase in E_{lg} and a decrease in E_{sl} of the Al−Mg−Sc system. It appears that adding the Sc element to Al−Mg−Sc increases the adsorption working of the melt on the BM surface, resulting in the melt spreading and adhering to the surface more readily. According to the literature,[22] when $E_{sl} < 0 < E_{lg}$, the addition of the Sc element to Al−Mg leads to an increase in the adsorption energy, while the contact angle decreases with decreasing tension. This is consistent with the calculation results in Section 3.2 and the experimental results in Section 3.3.

3.4. Molten Drop Transition Analysis. The current was maintained at 180 A, and the arc voltage was 20 V in the welding process. Therefore, the electromagnetic contraction force and the plasma flow force of the droplets on both wires were equal. High-speed photography and ImageJ were utilized to capture the transition process of the droplets and calculate the change in the size of the molten pool and droplets during one cycle.

The involution of the Al−Mg and Al−Mg−Sc wire molten droplets are displayed in Figures 5(a) and 6(a); the initial formation of the droplet ($t = 0$) and the droplet that has just come in contact with the molten pool are displayed in Figure 5(b) and 6(b); Figures 5(c) and 6(c) display the short-circuit transfer of the droplet to the molten pool; and Figure 5(d) and 6(d) show the end of one cycle, respectively. According to statistical results based on the 1 min stable welding process, the transition frequencies of the Al−Mg and Al−Mg−Sc wire droplets are about 85.70 and 76.92 Hz, respectively. The sizes of the melt pool during the transition of the two wires are shown in Table 3.

Table 3. Melt Pool of Al−Mg and Al−Mg−Sc Welding Wires (mm^2)

wires	initial	molten drop	disengage	terminate
Al−Mg	137.98	189.09	177.43	149.29
Al−Mg−Sc	160.73	190.21	184.83	162.21

Overall, the melt pool area during the droplet transition process shows a trend of first rising and then falling. When the droplet completes a transition cycle, the melt pool area is slightly larger than that at the initial transition of the droplet. As shown in Table 3 and Figure 7, in the process of molten droplet formation until the end of the transition, the melt pool area of the Al−Mg−Sc wire is moderately larger than that of the Al−Mg wire. This is attributed to the lower surface tension of the Al−Mg−Sc molten metal, which leads to good spreadability. The force that hinders the transfer of molten droplets is the surface tension and reaction force generated by the metal gas emitted from the molten pool.

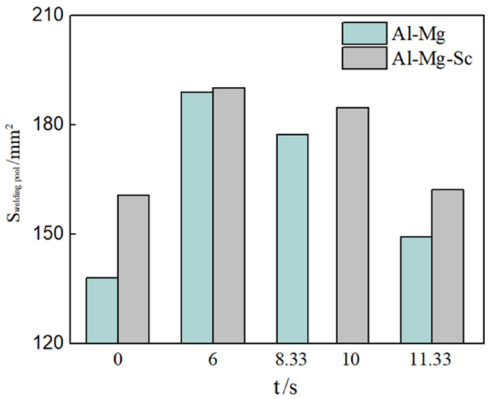

Figure 7. Comparison of the molten pool area during droplet transfer of two types of welding wires.

The molten drop formation of the Al−Mg and Al−Mg−Sc wires captured by high-speed photography is shown in Figure 8a,b. It marks the angle between the molten drop and the welding wire, and between the molten drop and the 7A52 BM surface, respectively. The angles of droplets with the wire tip BM for the Al−Mg wire and Al−Mg−Sc wire are 75.89 and 87.17°, respectively; the angles of the droplets with the 7A52 BM surface for the Al−Mg wire and Al−Mg−Sc wire are 33.4 and 29.45°, respectively; and the radii of the droplets of the Al−Mg wire and Al−Mg−Sc wire are 8.19 and 9.96 mm, respectively. After the addition of the Sc element, the radius of the droplet and the angle between the droplet and the wire are increased. The electromagnetic contraction force on the droplet can be expressed as follows according to the study of Liu[30] et al.

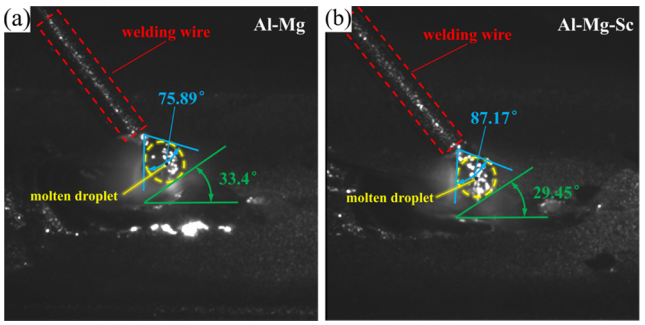

Figure 8. Angle of the molten droplet with the wire and 7A52 BM: (a) Al−Mg wire and (b) Al−Mg−Sc wire.

$$F_{em} = \frac{\mu_0 I^2}{4\pi} f_2 \tag{19}$$

$$F_{em} = \frac{\mu_0}{4\pi} I^2 \left[\frac{1}{4} - \left(\frac{3}{2} - \log 4 \right) \left(1 + \frac{c}{2R} \right)^{-2} \right] \tag{20}$$

where μ_0 is the dielectric permeability coefficient ($4\pi \times 10^{-7}$ $H \cdot m^{-1}$), I is the welding current, r_d is the radius of the wire, R is the radius of the droplet, θ is the angle of deflection of the droplet overhang, and c is the distance from the tip of the wire to the droplet, which has not yet been dislodged on the tip of the wire in the figure, so that $c = 0$.

According to eqs 19 and 20, when the welding parameters are the same, the electromagnetic contraction force on the two wires is mainly affected by the overhang angle and the radius of the molten drop. The larger the overhang angle of the droplet on the wire, the greater the electromagnetic contraction force. The droplet radius increases the volume of transition of the droplet to the molten pool, so the molten pool area of the aluminum−magnesium−scandium wire is more significant than that of the aluminum−magnesium wire. Adding the Sc element increases the overhang angle and radius of the droplet. Hence, adding the Sc element is conducive to the transition of the droplet to the molten pool.

The area change range of the Al−Mg wire melting pool in a cycle is larger than that of the Al−Mg−Sc wire, and the

https://doi.org/10.1021/acsomega.3c10018
ACS Omega 2024, 9, 14255−14261

transition frequency of molten droplets for the Al−Mg wire is higher than that of the Al−Mg−Sc wire. The projected area of the Al−Mg−Sc wire molten droplet is 15.21 mm^2, which is wider than that of the Al−Mg wire molten droplet (12.88 mm^2).

When the welding parameters are the same, the larger the overhang angle of the molten drop on the wire, the larger the electromagnetic contraction force on the molten drop; at the same time, the radius of the molten drop increases and the volume of the molten drop transitioning into the molten pool increases, so the area of the molten pool of the Al−Mg−Sc wire is larger than that of the molten pool of the Al−Mg wire. The electromagnetic contraction force is the force that promotes the transition of the molten drop; that is, the addition of the Sc element fosters the transition and spreading of the molten drop.

4. CONCLUSIONS

Al−Mg and Al−Mg−Sc ER5356 welding wires were adopted in this study; the effects of the Sc element on the wetting behavior of molten metal were studied, and the porosity of the deposited metal was investigated. The following conclusions can be drawn.

(1) The wetting angles of Al−Mg and Al−Mg−Sc welding wire on 7A52 BM are 17.2 and 12.4°, respectively. Adding the Sc element to the ER5356 welding wire reduced the melt wetting angle and the surface tension, thus increasing the adsorption working of the melt on the 7A52 BM surface, which improved the wettability and spreadability of the Al−Mg−Sc molten system.

(2) The pressure difference between the inside and outside of the melt for Al−Mg and Al−Mg−Sc welding wires were 0.086 and 0.106 MPa, respectively. The gas bubbles were easier to rupture and overflow from the Al−Mg−Sc molten pool. Therefore, the Al−Mg−Sc-deposited metal shows a lower porosity than the Al−Mg sample.

(3) The transition frequencies of the Al−Mg and Al−Mg−Sc wire droplets are about 85.70 and 76.92 Hz, respectively. The addition of the Sc element increases the electromagnetic contraction force on the droplet, increases the angle between the droplet and the tip of the wire, and decreases the angle between the surface and the molten pool, which promote the spreading of the droplet and thus increase the area of the molten pool. The increase of the electromagnetic contraction force also accelerated the transition frequency of the droplet.

■ ASSOCIATED CONTENT

Data Availability Statement

The raw/processed data required to reproduce these findings cannot be shared at this time due to technical or time limitations, and data will be available on request.

■ AUTHOR INFORMATION

Corresponding Author

Wenjing Yang − *Inner Mongolia Metal Material Research Institute, Baotou 014010, China; School of Materials Science and Engineering, Zhejiang University, Shenyang 110142, China;* orcid.org/0000-0001-9866-5286; Email: 9684960@qq.com

Authors

Haolin Zeng − *Inner Mongolia Metal Material Research Institute, Baotou 014010, China*

Zhuo Wang − *School of Materials Science and Engineering, Northeastern University, Shenyang 110016, China*

Donggao Chen − *Inner Mongolia Metal Material Research Institute, Baotou 014010, China*

Hua Ding − *School of Materials Science and Engineering, Northeastern University, Shenyang 110016, China*

Liangchao Ma − *Inner Mongolia Metal Material Research Institute, Baotou 014010, China*

Yu Lu − *Inner Mongolia Metal Material Research Institute, Baotou 014010, China*

Complete contact information is available at: https://pubs.acs.org/10.1021/acsomega.3c10018

Author Contributions

[‖]H.Z. and Z.W. contributed equally to this work and should be considered cofirst authors; H.Z. and Z.W.: experiment, calculation, investigation, formal analysis, writing—original draft, review, editing, and revision; D.C. and H.D.: supervision; W.Y.: conceptualization, experiment, calculation, writing—translation, review, and editing; L.M. and Y.L.: depositing experiment and specimen preparation. All authors have approved the manuscript that is enclosed. The authors declare that the work described is original research that has not been published previously and is not under consideration for publication elsewhere, in whole or in part.

Notes

The authors declare no competing financial interest.

■ ACKNOWLEDGMENTS

This work was supported by the National Natural Science Foundation of China (U2241248).

■ REFERENCES

(1) Zhou, G. X.; Lang, Y. J.; Hao, J.; Liu, W.; Wang, S.; Qiao, L.; Chen, M. Interface analysis of 7B52 Al alloy laminated composite fabricated by hot-roll bonding. *Trans. Nonferrous Met. Soc. China* **2016**, *26* (5), 1269−1275.

(2) Liu, X.; Jia, R. L.; Cheng, W. H.; Zhang, H. X.; Tian, J.; Zhai, X. W. Influence of the second phase on relative fracture behavior of friction stir welded 7A52 aluminum alloy. *Mater. Today Commun.* **2022**, *33*, No. 104215.

(3) Chao, C.; Chen, F.; Zhang, H. Surface Nanocrystallization of 7A52 Aluminum Alloy Welded Joint by Aging and Ultrasonic Impact Compound Treatment. *Rare Met. Mater. Eng.* **2018**, *47* (9), 2637−2641.

(4) Hu, Y.; Wu, S.; Shen, Z.; Cao, H. T.; Zhong, X. L.; Withers, P. J. Fine equiaxed zone induced softening and failure behavior of 7050 aluminum alloy hybrid laser welds. *Mater. Sci. Eng., A* **2021**, *821*, No. 141597.

(5) Feng, Y. H.; Chen, J. H.; Wei, Q.; Wang, K. H. Microstructure and mechanical properties of aluminium alloy 7A52 thick plates welded by robotic double-sided coaxial GTAW process. *Mater. Sci. Eng., A* **2016**, *673*, 8−15.

(6) Deng, Y.; Peng, B.; Xu, G. F.; Pan, Q. L.; Yin, Z. M.; Ye, R.; Wang, Y. J.; Lu, L. Y. Effects of Sc and Zr on mechanical property and microstructure of tungsten inert gas and friction stir welded aerospace high strength Al−Zn−Mg alloys. *Mater. Sci. Eng., A* **2015**, *639*, 500−513.

(7) Fu, L.; Peng, Y. Y.; Huang, J. W.; Deng, Y.; Yin, Z. Microstructures and mechanical properties of Gas Tungsten Arc Welded joints of new Al−Mg−Sc and Al−Mg−Er alloy plates. *Mater. Sci. Eng., A* **2015**, *620*, 149−154.

(8) Tomus, D.; Qian, M.; Brice, C. A.; Muddle, B. C. Electron beam processing of Al−2Sc alloy for enhanced precipitation hardening. *Scr. Mater.* **2010**, *63* (2), 151−154.
(9) Liu, F. Y.; Yang, B.; Sun, H. F.; Wang, H. Q.; Tan, C. W.; Wang, G. D.; Chen, B. Mechanism investigation for the influence of laser power on droplet transfer behaviors in laser-MIG hybrid welding. *Opt. Laser Technol.* **2023**, *157*, No. 108750.
(10) Kramer, L. S.; Tack, W. T.; Fernandes, M. T. Scandium in aluminum alloys. *Adv. Mater. Processes* **1997**, *152* (4), 23−24.
(11) Ding, J.; Zhang, P.; Li, X.; Wang, L. S.; Liao, W. Z.; Huang, L. X.; Xia, X. C. Microstructure and thermal stability evolution behavior of Sc-containing A356.2 aluminum alloy under cyclic thermal exposure conditions. *Mater. Sci. Eng., A* **2018**, *723*, 165−173.
(12) Algendy, A. Y.; Liu, K.; Rometsch, P.; Parson, N.; Chen, X. G. Effects of AlMn dispersoids and Al_3(Sc,Zr) precipitates on the microstructure and ambient/elevated-temperature mechanical properties of hot-rolled AA5083 alloys. *Mater. Sci. Eng., A* **2022**, *855*, No. 143950.
(13) Yan, K.; Chen, Z. W.; Zhao, Y. N. Morphological characteristics of Al_3Sc particles and crystallographic orientation relationships of Al_3Sc/Al interface in cast Al-Sc alloy. *J. Alloys Compd.* **2020**, *861*, No. 158491.
(14) Liu, X.; Guo, H.; Xue, J. L.; Wang, Z. J.; Zhang, Y. N.; Li, X. Microstructure and mechanical properties of as casted Al-Si-Sc-Ce alloys prepared by molten salt electrolysis with varied cooling rate. *J. Alloys Compd.* **2023**, *947*, No. 169703.
(15) Cavanaugh, M. K.; Birbilis, N.; Buchheit, R. G.; Bovard, F. Investigating localized corrosion susceptibility arising from Sc containing intermetallic Al_3Sc in high strength Al-alloys. *Scr. Mater.* **2007**, *56* (11), 995−998.
(16) Wang, R.; Jiang, S.; Chen, B.; Zhu, Z. X. Size effect in the Al_3Sc dispersoid-mediated precipitation and mechanical/electrical properties of Al-Mg-Si-Sc alloys. *J. Mater. Sci. Technol.* **2020**, *57* (22), 78−84.
(17) Deng, A. L.; Chen, H.; Zhang, Y. B.; Liu, Y.; Yang, X. Y.; Zhang, B. X. Effect of filler materials on the porosity formation of aluminum alloy by laser welding with filler wire. *Opt. Laser Technol.* **2023**, *159*, No. 109000.
(18) Keene, B. J. Review of data for the surface tension of pure metals. *Int. Mater. Rev.* **1993**, *38* (4), 157−192.
(19) Wu, T.; Wu, P. An entropic Young's equation approach for magneto-wetting modeling. *Extreme Mech. Lett.* **2021**, *43*, No. 101210.
(20) Molina, J. M.; Voytovych, R.; Louis, E.; Eustathopoulos, N. The surface tension of liquid aluminium in high vacuum: the role of surface condition. *Int. J. Adhes. Adhes.* **2007**, *27* (5), 394−401.
(21) Yan, X. W.; Qiu, T.; Zhang, Z. Z. *Double Sphero-crown Wetting Model and Wettability Characterization Factor λ*; Lanzhou University of Technology, 2006.
(22) Wang, X. W.; Jia, L.; Dang, C. The wetting transition of low surface tension droplet on the special-shaped microstructure surface. *Colloid Interface Sci. Commun.* **2022**, *50*, No. 100649.
(23) Río, O.; Neumann, A. W. Axisymmetric Drop Shape Analysis: Computational Methods for the Measurement of Interfacial Properties from the Shape and Dimensions of Pendant and Sessile Drops. *J. Colloid Interface Sci.* **1997**, *196* (2), 136−147.
(24) Pierson, J. L.; Magnaudet, J. Inertial settling of a sphere through an interface. Part 2: Sphere and tail dynamics (accepted version). *J. Fluid Mech.* **2018**, *835*, 808−851.
(25) Atkins, P.; Paula, J. D. *Atkins' Physical Chemistry*, 8th ed.; Oxford University Press: Oxford, U.K., 2006; pp 335−350.
(26) Li, J. G.; Coudurier, L.; Eustathopoulos, N. Work of adhesion and contact-angle isotherm of binary alloys on ionocovalent oxides. *J. Mater. Sci.* **1989**, *24* (3), 1109−1116.
(27) Takeuchi, A.; Inoue, A. Classification of Bulk Metallic Glasses by Atomic Size Difference, Heat of Mixing and Period of Constituent Elements and Its Application to Characterization of the Main Alloying Element (Overview). *Mater. Trans.* **2005**, *46* (12), 2817−2829.
(28) Zhang, R. F.; Zhang, S. H.; He, Z. J.; Jing, J.; Sheng, S. H. Miedema Calculator: A thermodynamic platform for predicting formation enthalpies of alloys within framework of Miedema's Theory. *Comput. Phys. Commun.* **2016**, *209*, 58−69.
(29) Cong, X. S.; Shen, P.; Wang, Y.; Jiang, Q. C. Wetting of polycrystalline SiC by molten Al and Al-Si alloys. *Appl. Surf. Sci.* **2014**, *317*, 140−146.
(30) Liu, S.; Liu, F.; Zhang, H.; Shi, Y. Analysis of droplet transfer mode and forming process of weld bead in CO_2 laser−MAG hybrid welding process. *Opt. Laser Technol.* **2012**, *44* (4), 1019−1025.

https://doi.org/10.1021/acsomega.3c10018
ACS Omega 2024, 9, 14255−14261